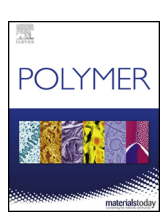


Contents lists available at ScienceDirect

Polymer

journal homepage: www.elsevier.com/locate/polymer



Topological defects in tubular network block copolymers

Xueyan Feng, Hua Guo, Edwin L. Thomas*

Rice University, Houston, TX, USA



HIGHLIGHTS

- Large volume reconstruction of the tubular double gyroid block polymer structure.
- Discovery and classification of topological defects in the double gyroid network.
- Impact of defects on physical properties for the double gyroid structure was discussed.

ARTICLE INFO

Keywords:
Network breaks
F defects
Intra-net donuts
Intra-net loops
Network bridges
Properties of 3D network materials

ABSTRACT

Materials based on the double gyroid multicontinuous tubular structure can exhibit exotic properties due to the unique 3D network structure. The nature, frequency and potential influence of topological defects present in the interpenetrating gyroid networks on various physical properties is an open question. We examined a polystyrene – polydimethylsiloxane diblock copolymer possessing the double gyroid morphology in order to identify and classify the types of topological defects present. The large volume reconstructions were made by sequentially ion beam milling and low voltage electron beam imaging. Different types of local point-like topological defects were found including node functionality defects, network breaks and network-network joints (bridges) as well as two types of intra-network loop defects. Such topological defects will influence properties ranging from charge and mass transport, to wave propagation and band gaps, and battery performance in materials with the gyroid structure.

1. Introduction

Many self assembled block polymer (BCP) microdomain structures having highly complex patterns, have been discovered in the past few decades [1–5]. The normal tools for determination of the 3D structure of soft materials, small angle X-ray scattering (SAXS) and transmission electron microscopy (TEM) while able to identify the 3 canonical BCP structures (spheres, cylinders, lamellae [6]) can be inadequate for conclusive identification of complex tubular morphologies and especially for revealing details of the local domain geometry, topology and defects. Moreover, as block polymer materials take on more roles as key components in various technological applications, understanding the nature of defects in these unique structures and their influence on the corresponding material properties is an important endeavor [7–10].

Materials comprised of tubular networks with double gyroid (DG) symmetry have many unique and intriguing properties due to the percolated nature of the two networks in all 3 directions (i.e. multicontinuous structures) [2]. Such tubular BCPs possess (nano)composite functional property attributes stemming from the nature of each

component block and from their small length scale, mutual arrangement and in particular, the 3D continuity of each type of domain. For example, a superior membrane material would contain a continuous glassy network for mechanical stiffness and strength [11-13] in order to support the applied pressure and a soft rubbery continuous phase for high selectivity, good solubility and excellent diffusivity of ions/gas(es) across the membrane [14]. Additionally, researchers have used DG systems as templates for ordering nanoparticles and for making metallic or ceramic nanoporous composites [15-17]. Moreover, a number of researchers have used various methods to remove one of the components of a double gyroid structure resulting in periodic porous materials that can in turn be filled with metals via electroless deposition [18] or filled with a ceramic by the sol-gel process [19] or even turned into a "gyroidal battery" by fabricating a high temperature graphitic and lithiated (cathode) network followed by creation of a metallic network (anode) enabling extraordinary fast recharging via exploiting the 3D multiphase continuity and the nano length scale of the structure [20]. Optical properties of the gyroid phase are also unique. A single gyroid network possesses a large complete optical band gap [21] and the band

E-mail address: elt@rice.edu (E.L. Thomas).

^{*} Corresponding author.

structure of the double gyroid exhibits Weyl points that enable topologically protected propagation modes [22–24].

SAXS provides information about structural order via the distribution of scattered intensity in reciprocal space but cannot yield precise real space information about the nature of defects. TEM images are projections of thin specimens along a specific direction and can reveal the presence of defects such as dislocations and grain boundaries in the simpler domain packing structures [25-29]. Tilting about an axis and obtaining multiple TEM images can help decipher the 3D domain geometry e.g. the packing of spheres onto a bcc lattice via 3 systematic views of a single grain along the [100], [110], and [111] directions [30]. A small set of images taken at different degrees of tilt can also reveal the nature of grain boundaries in 1D periodic lamellar structures as twist [26] or tilt [25] boundaries. However, to truly characterize the detailed nature of a complex microdomain structure such as the DG or the double diamond (DD) and to study defects in such tubular microdomain structures with high fidelity, 3D tomography via the back projection of over one hundred systematic TEM images acquired over a large range of tilt angles is necessary [31,32]. However, even TEM tomography has limitations, arising from missing information due to the required small sample thickness, the limited possible range of tilt angles for the set of image projections, or distorted information due to morphological disturbances to the sample occurring from microtomy and accumulated radiation damage during observation [31]. Moreover, TEM tomography usually results in rather small total reconstructed volumes (a few (~10) unit cells) that makes it difficult to properly identify and characterize defects and lacks the statistics to reliably assess the relative concentration of individual defects in the material. While 3D TEM tomograms have been constructed in order to examine the epitaxial relationships during order-order transitions to/from the DG phase from/to the lamellar, cylindrical and twisted cylinder phases [33-35], to date, topological defects within network phases are rather unexplored.

Imperfections in ordered soft matter range from thermal fluctuations to point, line and surface defects that break symmetry at the local scale [36]. Well below the disordering transition to the isotropic phase, defects, while even relatively dilute, can play an outsized role in determining the properties of the material. Defect studies of block copolymers with 3D symmetries (i.e. the spherical phases and tubular phases) are rare. While Hashimoto et al. [37,38] studied defects in bulk bcc spherical phases, Chaikin et al. [39] and Kramer et al. [40] investigated defects in mono/few layer thin spherical domain films, there appear to be no studies of defects in the newly found Frank-Kasper and closely related quasi-crystalline spherical phases [41,42]. The DG, DD,

and O⁵² and O⁷⁰ phases [2], the so called tubular network microdomain phases, are comprised of one or more 3D continuous tubular networks embedded in a continuous matrix (hence a structure that is at least bicontinuous). These networks have novel domain shapes and symmetries with various types of network connectivity and therefore are topologically complex. Topological defects in a material such as the DG can either create additional phase continuity or break phase continuity or cross-couple the two otherwise independent (and enantiomorphic) network domains. Defects produce stress and strain fields that interact with other stress fields arising from other defects, nanoparticle additives as well as internal boundaries/external surfaces.

The occurrence of defects in BCPs can arise due to local errors occurring during self assembly from solvent evaporation at constant temperature (passing through the disorder-order concentration) or from cooling the sample from an isotropic high temperature melt state (passing through the disorder-order temperature). The appearance of defects happens during such transformations and if samples are annealed well above the Tg of the each block, the defect concentration can be lowered via their diffusive migration and mutual annihilation. An additional source of defects can arise from material processing under the application of a strong field (e.g. flow or electric) that can induce network domain deformation and overall anisotropy of the sample via texturing [5,13]. Depending on their energy of formation, some types of (point) defects may be present at equilibrium and their concentration would increase with temperature. All types of defects in a sample having a Tg well above room temperature are essentially trapped.

There have been many 3D TEMT reconstructions of block copolymers, dating from the first effort on hexagonally packed cylinders by Spontak et al., in 1988 [43]. Researchers occasionally found evidence for defects but the typical quality of the reconstruction and the small size of the reconstructed volume limited the ability to elucidate the details of the defects while the main effort was directed towards imaging the overall domain packing schemes. Recent research has sought to establish relationships between adjacent BCP phases in order-order transitions (OOT) [33–35,44–48]. Some TEMT reconstructions show a few local defects at the boundary between two phases at an OOT [33–35,47].

The gyroid (G) is a triply periodic minimal surface discovered by Schoen [49]. The G surface divides space into two regions of 50 vol per cent. The DG network structure found in block polymers consists of two independent, opposite handed, interpenetrating (10, 3)-a networks with 3 coordinated nodes embedded in a matrix [50]. These networks are located on opposite sides of Schoen's G surface. The cubic space group of the double gyroid is $Ia\bar{3}d$. The set of symmetries include inversion

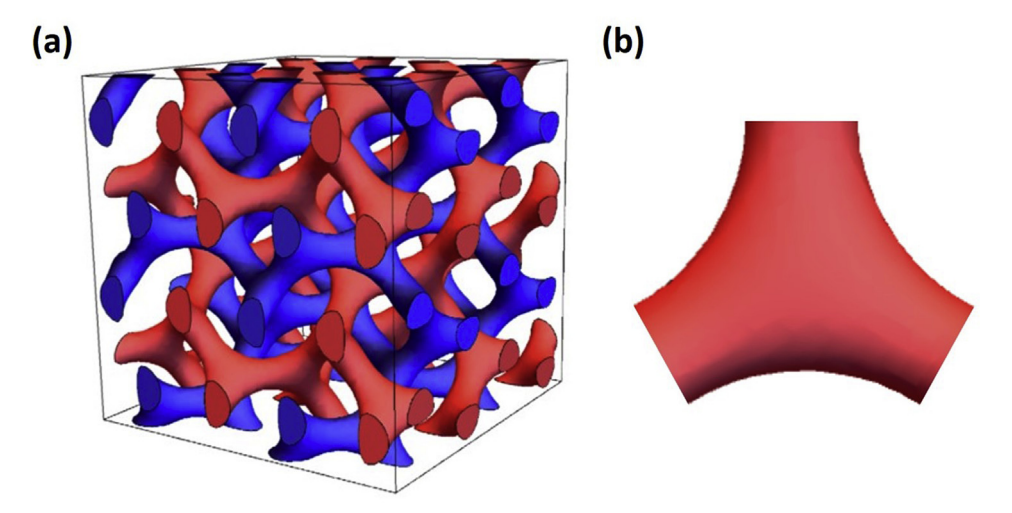


Fig. 1. (a) Simulated $2 \times 2 \times 2$ unit cell volume of a DG structure using a level set equation showing the two interpenetrating networks: red (right handed) and blue (left handed); (b) the basic building block is a 3 strut node region with inter strut angle of 120° .

centers, 2, 3 and 4 fold screw axes as well as glide planes. There are no mirror planes and the two independent networks are enantiomorphic. For a diblock DG, the basic building block of the structure is a 3 strut node region (see Fig. 1). There are 16 such equivalent positions in the unit cell (Wyckoff site 16b). An inversion point is located between pairs of nearby nodes, one node from each of the two types of networks. All struts are of equal length, are oriented along the < 110 > directions and meet in threes with 120° angles between adjacent pairs of struts. The dihedral angle between pairs of 3 strut nodes is defined by a set of 5 struts and is \pm 70.5 CW or CCW depending on the network chirality D or L [16,51]. Single and double gyroid morphologies have been discovered in a number of biological systems [52] as well as surfactant/ oil/water systems [53] and in numerous block polymers [50,54-56]. The frequent appearance of the DG tubular network structure over all others is attributed to the low interfacial area and relative homogeneity of the local packing environments partitioned into domains by the intermaterial dividing surface (IMDS). The distances from the skeletal graph (centerline of a network) to the IMDS as well as the distances from the IMDS to the infinite periodic minimal surface (Schoen's G surface) are relatively uniform so as to accommodate the near monodisperse nature of each block in the copolymer [57].

The first 3D TEMT reconstruction of the DG structure [58] was published by Spontak et al. analyzing a blend of two diblocks in 1996, followed in 1997 [59] by more detailed, better resolution work on a triblock also with the DG structure. Subsequently, in a collaboration with the Hashimoto group in 2000, the 1997 structural data was used to measure the variation of the local surface curvature of the IMDS separating the respective domains [32]. Jinnai et al. [58] then further identified topological point defects in the form of network nodes with four (9%) and five (1.3%) functionality present in the 3D TEM tomogram. This relatively high number of node defects was consistent with their estimates of the rather low average Euler characteristic $(\chi = -12.1)$ and genus $g = 1 - \chi/2$ (g = 7.1) of the average experimental unit cell compared to the ideal reference values of $\chi = -16$ and g = 9 for the defect free DG network. Studies of BCPs with the DG structure have occasionally mentioned defects or shown images containing defects without detailed comment. The only other TEMT study of BCPs that addressed defects was that of a metallic network alternating double gyroid structure made by blending a triblock terpolymer with metal nanoparticles in order to template the additives into one specific single gyroid network [16]. The chirality of a grain of the metal containing network was assessed by measurement of the dihedral angle between adjacent nodes. Nodes with different functionalities were mentioned but no concentrations were discussed. The dihedral analysis pointed to a single network handedness but the extremely wide distribution of dihedral angles indicated very significant distortions of the

Non-local defects such as grain boundaries are evident in TEM images of the DG, for example, a PS-PI diblock DG structure [60]. Many images in the literature purported to be from the DG phase show relatively poor long range order and Fast Fourier transforms of such images show broad and noncircular halos corresponding to the various Bragg peaks ({211}, {220} etc) indicative of the lack of truly long range ordering of the microdomains as well as apparent sample anisotropy, making characterization of defects in such samples problematic. Computational studies of defects in small molecule systems having the DG phase were conducted by Harting et al. [61]. They used a lattice Boltzmann method and pattern recognition algorithms to study defects in a ternary amphiphilic fluid that forms the DG phase. Their work included a simulation of an edge dislocation dipole (their Fig. 2) with the dislocation line oriented along the [001] direction with a Burgers' vector of a/2[100]. Harting et al. also mention topological point defects without elaboration [61]. The mobility of defects in liquid crystal versions of the DG will be much higher than in the polymer case due to the softer molecular potentials.

Natural systems having a single gyroid (SG) structure, as occurs for

example in butterfly wings [62], have also been studied. Ptychographic imaging using X-rays showed oriented crystal growth and sharp, high angle grain boundaries as well as low angle boundaries comprised of edge dislocations. How such defects that form in a growing biological system relate to a synthetic block copolymer undergoing a phase transformation to the DG phase either via an order-order or disorder-order transition is unknown at present. Here in this report, taking advantage of the newly developed slice and view scanning electron microscopy (SVSEM) tomography method for high-fidelity 3D reconstruction of complex ordered nano structures [57], a number of different types of topological defects within a polystyrene-b-poly-dimethylsiloxane (PS-PDMS) DG network have been examined and classified.

2. Experimental

The PS-PDMS diblock we study has a PS block of 43.5 kg/mol and PDMS block of 29 kg/mol for a total number average molecular weight of 72.5 kg/mol and a polydispersity of 1.04. The two PDMS networks are each approximately 20 vol per cent. The sample was cast from toluene and is the same BCP sample studied in Ref. [63]. The spacing of the d₂₁₁ SAXS peak is 54 nm that corresponds to a cubic unit cell lattice parameter of 132 nm. 3D reconstruction is accomplished with SVSEM technique [64,65] using a Helios 660 dual beam FIB/SEM. A stack of secondary electron images is made by a 30 keV Ga + ion beam sequentially ion milling away thin (~3 nm) slices of the sample. We then image each newly exposed surface via normal incidence secondary electron microscopy operating at low voltage (~1 KeV) to restrict the signal to the near surface region [66,67]. Many hundreds of cycles of slice and view result in 3D tomographic reconstructions over specimen volumes containing thousands of unit cells. By employing a BCP with one block having a different atomic number species (such as silicon in PS-PDMS), the intrinsic image contrast is sufficiently strong so there is no need of selective staining that can alter the sample dimensions and will also be depth dependent. We drill deep holes along the direction normal to electron beam observing surface using the ion beam to create local fiducial markers for image registration and Avizo and ImageJ software for image manipulation such as segmentation and determination of the skeletal graphs [68] (more experimental details are given in the SI).

3. Results and discussion

Wells [69] in his book on "Three Dimensional Nets and Polyhedra," classified regular 3D networks depending on the number of nodes in the smallest closed loop and also the node functionality. Thus, the (10, 3)-a network has as its smallest closed path, a 10 node (and 10 connecting strut) loop with each node of the loop having a functionality of 3. All nodes are equivalent and are comprised of 3 coplanar "struts" (aka graph edges) of equal length. In noncrystalline BCPs, the order is not in the locations of the atoms or so much the conformations of the molecules but in the nature of the IMDS separating the component blocks. A thinning algorithm when applied to each IMDS defines the basic skeletal graph corresponding to the two enantiomorphic (10–3)-a network graphs. Simple ball and stick models are shown in Fig. 2a and b for right and left handed skeletal loops alongside the experimental PS-PDMS IMDS that surrounds these loops that have been cut out of the slice and view reconstruction. The match is quite good (see Animations S1 and S2 in the SI).

Supplementary video related to this article can be found at https://doi.org/10.1016/j.polymer.2019.01.085

Defects are regions in the material where the symmetry is broken and elastic stresses arise due to the disruption of the orderly periodic packing. In tubular network block copolymer assemblies, topological defects can disrupt the network continuity by breaking of normally connected struts or by making additional strut connections within a

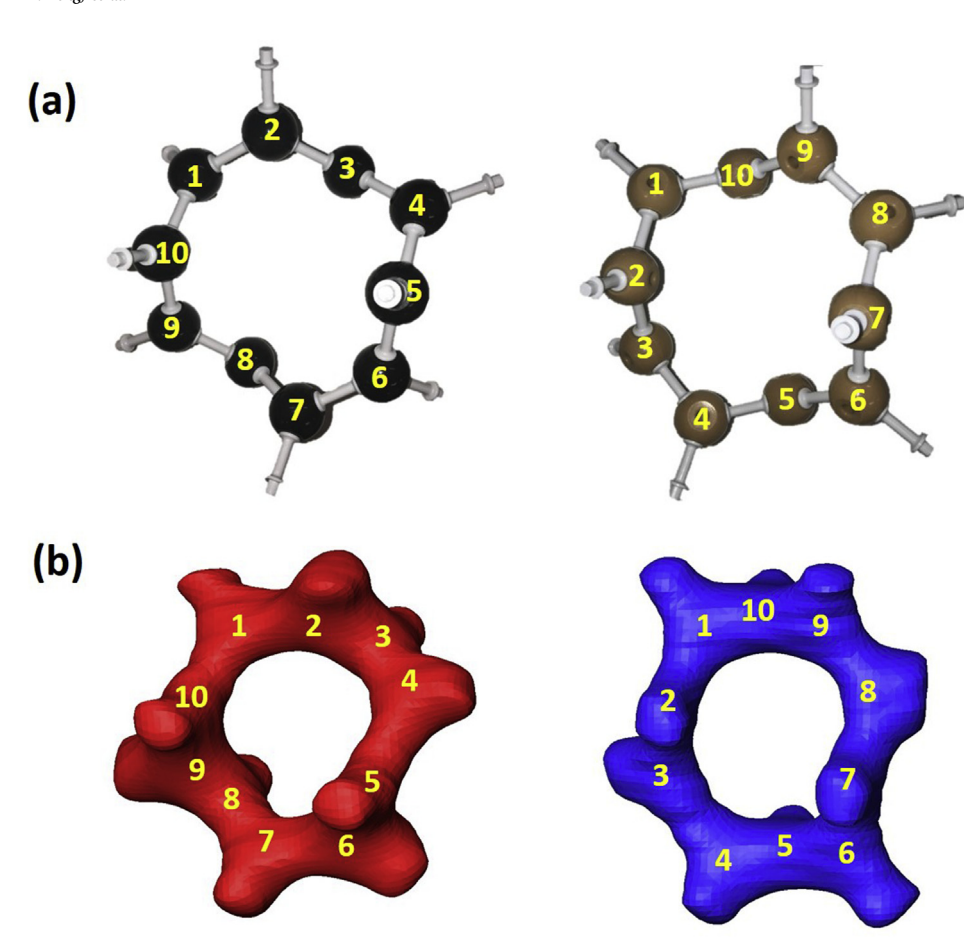


Fig. 2. (a) Chemistry models (skeletal graph loops) of right (black) and left (brown) handed (10, 3)-a loops, (b) cropped regions from SVSEM experimental reconstruction: right (red) and left (blue) handed PS-PDMS DG IMDS structures. The location of the internal node positions in the fundamental (10,3)-a topological loops are denoted by the numbers.

network or across networks. Due to the fact that in a diblock copolymer, the PS and PDMS blocks are covalently connected, the sample composition has to average to the value of the copolymer (i.e. 60/40 vol ratio) over a unit region (such as a unit cell or small set of cells containing defect(s)). Thus, the distances between the various domain-domain interfaces around any defect cannot be too small nor too large, due to the fixed size of the block polymer molecules, their desire to assume high entropy conformations while minimizing interfacial area and the requirement to fill space with a uniform density. Since the composition is conserved, the PDMS material that would have normally been in the red or blue strut regions (Fig. 1a, see the simulated red and blue networks) that is missing (strut breaks) or any additional extra struts (bridges) has to be relocated from/to nearby red/blue networks. For example, at a break, some of the PS matrix domain (shown as transparent) must relocate into what was previously the colored PDMS network domain and the PDMS blocks that formerly occupied the connected PDMS strut region have to be incorporated into thickening and rounding the surrounding, now terminated PDMS struts.

To locate defects, we surveyed SE images of sample regions searching for local departures from the periodic contrast patterns and also viewed the skeletal graphs of 3D reconstructions looking for disruptions from the ideal ordered graphs. A SE image of a region of the PS-PDMS sample containing a topological defect is shown in Fig. 3, where there are deviations from the repetitive pattern of domain contrast. In order to decipher the nature of such defects, 3D tomograms of these regions are constructed. Fig. 4a is an example of local break defects in both of the networks. Each location where the connecting strut would normally reside shows a pair of blunted PDMS struts with the gap filled with PS. Fig. 4b shows defects where the local node functionality is 4 or 5. In order to better appreciate the 3D nature of these defects, rotational videos of each of the defects are available in the SI

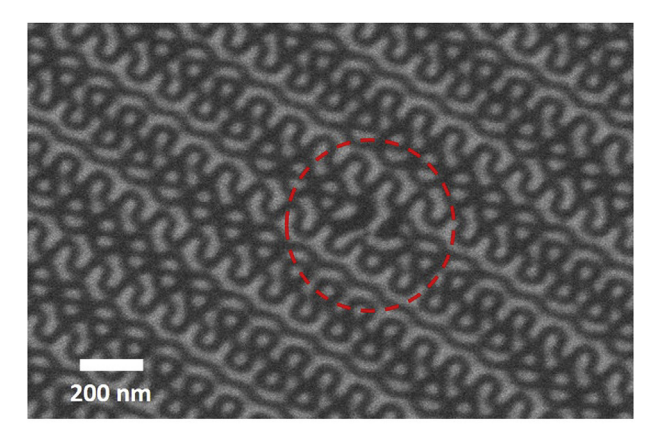


Fig. 3. 2D SEM image showing a local defect (dashed red circle). The defect region breaks the symmetry of the surrounding repetitive pattern. The PDMS domains are bright and the PS matrix is dark.

(Animations S3 & S4). The f ;= 4 node displays some thickness variation of the individual struts and the angles between adjacent pairs of struts vary from a high of 123° to a low of 86° . The f = 5 node also displays struts with varying thicknesses and the angles between adjacent pairs of struts vary from a high of 143° to a low of 77° . The variation of the angles between pairs of struts on a given defect node results from the variation of the local environment within the structure as the various struts distort in order to connect into one of the surrounding gyroid networks.

Supplementary video related to this article can be found at https://doi.org/10.1016/j.polymer.2019.01.085

The f defects lead to defect loops that can form within a single

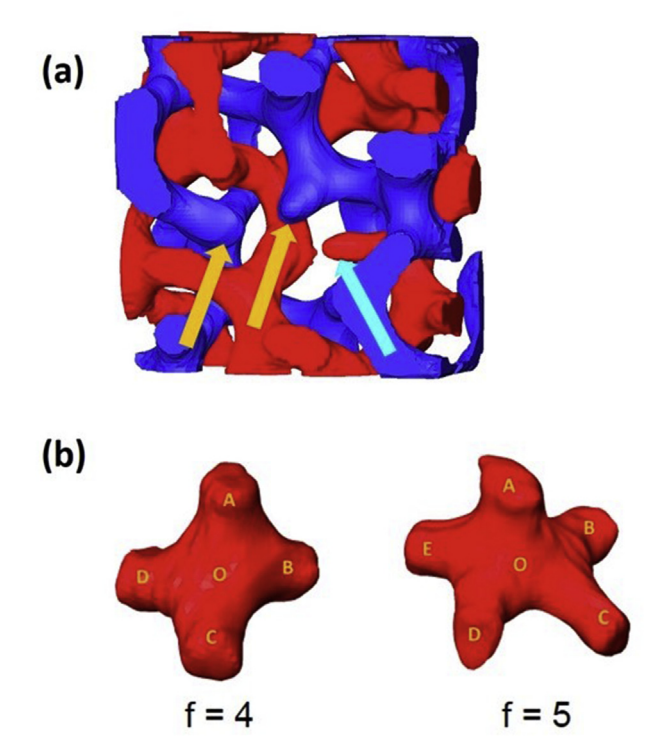


Fig. 4. (a) Network break defects showing disconnection of the blue network (orange arrows) and disconnection of red network (light blue arrow); (b) f=4 node and f=5 node cropped from the experimental SVSEM reconstruction.

network or across the two networks. We have identified small loops within a single network having either 5 or 6 nodes that define a smaller interior hole; we term this type of defect, an intra-net "donut." Because the donut loops are small (with typical inner hole diameter $\sim 20 \text{ nm}$), their interior hole is too tiny to accommodate the threading-through of the second network and this in turn perturbs the topology of the second network. Examples of three different "donut" type defects are shown in Fig. 5 (rotational videos of these "donut" type defects are available in the SI (Animation S5-7)) We call the 5 node donut loops 5-4,34 and 5-4²,3³ defects while the 6 node donut loop is termed a 6–4,3,4,3³ defect to indicate, adapting from Wells, the number of nodes (struts) in the loop as well as the node functionality and sequence. Thus, a 5 donut has 5 nodes with 1 or 2 adjacent nodes with 4 coordination, while the 6 donut loop has 6 nodes with the two f = 4 nodes separated by a f = 3node. Due to both network strain and topology, such donuts tend to appear in a cluster with donut defects in both of the respective networks. In Fig. 6, we show a cluster of five donut defects comprised of 2 red donuts and 3 blue donuts and these defects serve to accommodate a tilt of about 8° across the gyroid grain.

Supplementary video related to this article can be found at https://doi.org/10.1016/j.polymer.2019.01.085

Defects with f=4 or f=5 node functionality can also participate in larger *intra-net loop defects* (with typical inner hole diameter ~ 75 nm) containing 7, 8 or 9 nodes. The interiors of these loops are sufficiently large to allow threading-through of the second network. Fig. 7 shows a region within a grain with f=4 and f; = 5 defects and 3 examples of associated intra-net defect loops of 7-5,3,4,3 4 ; 8–4,3 2 ,4,3 4 and 9–4, 3 8 (Animations S8–S10). This cluster of defects leads to an approximate 5 $^\circ$ tilt of the two portions of the grain on either side of the defect array. The spatial distribution of the 25 total f=4 nodes and the single f=5 node defect are best shown in the skeletal graphs in Fig. 7b. Examining the surrounding ~ 100 unit cells (1722 nodes), we find there are 98.49% f=3 nodes and only 1.45% f=4 nodes and a single f=5 node.

Supplementary video related to this article can be found at https://doi.org/10.1016/j.polymer.2019.01.085

A *bridge* defect connecting the two otherwise independent networks is shown in Fig. 8 (see Animation S11, SI). Here a single strut from a red loop $(9-4,3,4,3,4,3^3,4)$ merges with the surrounding blue network to form a smaller loop $(8-4,3^7)$. Such bridging defects are obviously critical in applications such as the 3D gyroidal battery, where one network is employed as the cathode and the other the anode such that a bridging defect could short a portion of the battery (see Fig. 9).

Supplementary video related to this article can be found at https://doi.org/10.1016/j.polymer.2019.01.085

The relatively localized region of distortion/elastic stress around all the various observed defects suggests that their energies of formation are not overly large. Rapid formation of the DG phase by either fast solvent evaporation (along with shrinkage stresses) or by deep thermal quenching will increase defect content. Systematic observation of the number and nature of the defects as a function of solvent evaporation rate, quench depth and degree of segregation, sample temperature relative to T_g and T_{ODT}, and any imposed flow during the processing will be revealing concerning defect formation energies, and their mutual interactions. It will be fascinating to follow the 3D detailed mechanisms of defect annihilation and/or defect assembly (such as to form low angle grain boundaries) during various types of annealing conditions as well as under the influence of applied external fields (e.g. electric, oscillating shear etc.), although since SVSEM is a destructive technique, sets of similar defects will need to be monitored over the annealing procedure.

It is obviously important for applications of DG and other tubular networks to both control and minimize the number of the various kinds of defects. As mentioned previously, using a TEMT 3D reconstruction, Jinnai et al. found a surprisingly high value of over 1 functionality defect per average unit cell [70]. In the present PS-PDMS material, the defect concentration is much lower. Indeed, Fig. 9 shows a 3D SVSEMT reconstruction of a $5 \times 5 \times 5$ unit cell volume containing

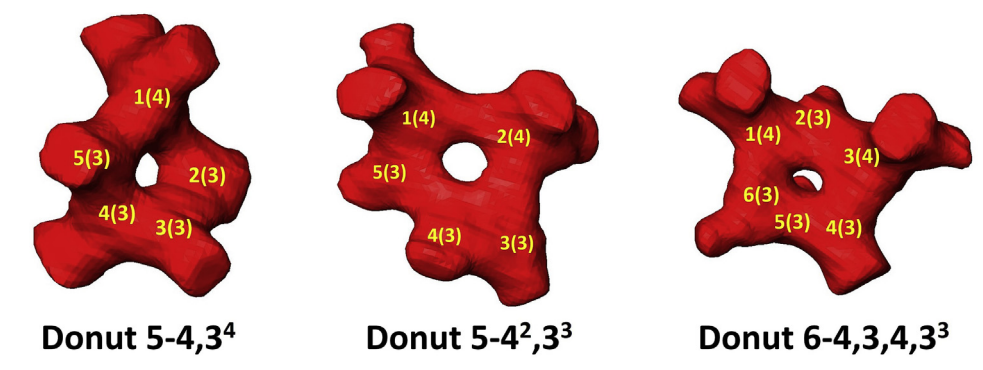


Fig. 5. (a) Three intra-donut loop defects with $5-4,3^4$ loop, $5-4^2,3^3$ loop and $6-4,3,4,3^3$ loop. The two yellow numbers at each node in the figures represent the node number and node functionality. Thus, a 3(4), indicates that node number 3 has functionality of 4 (f = 4).

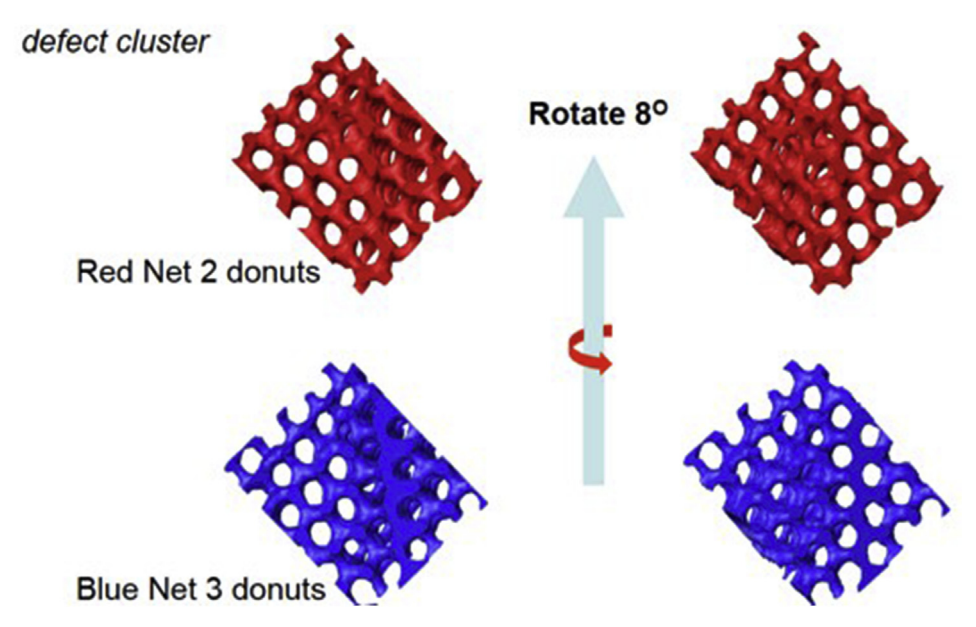


Fig. 6. A defect cluster comprised of a group of 5 total donut loops. Topological defects occur in both the red and in the blue networks and lead to an approximate 8° of tilt of the two portions of the DG grain.

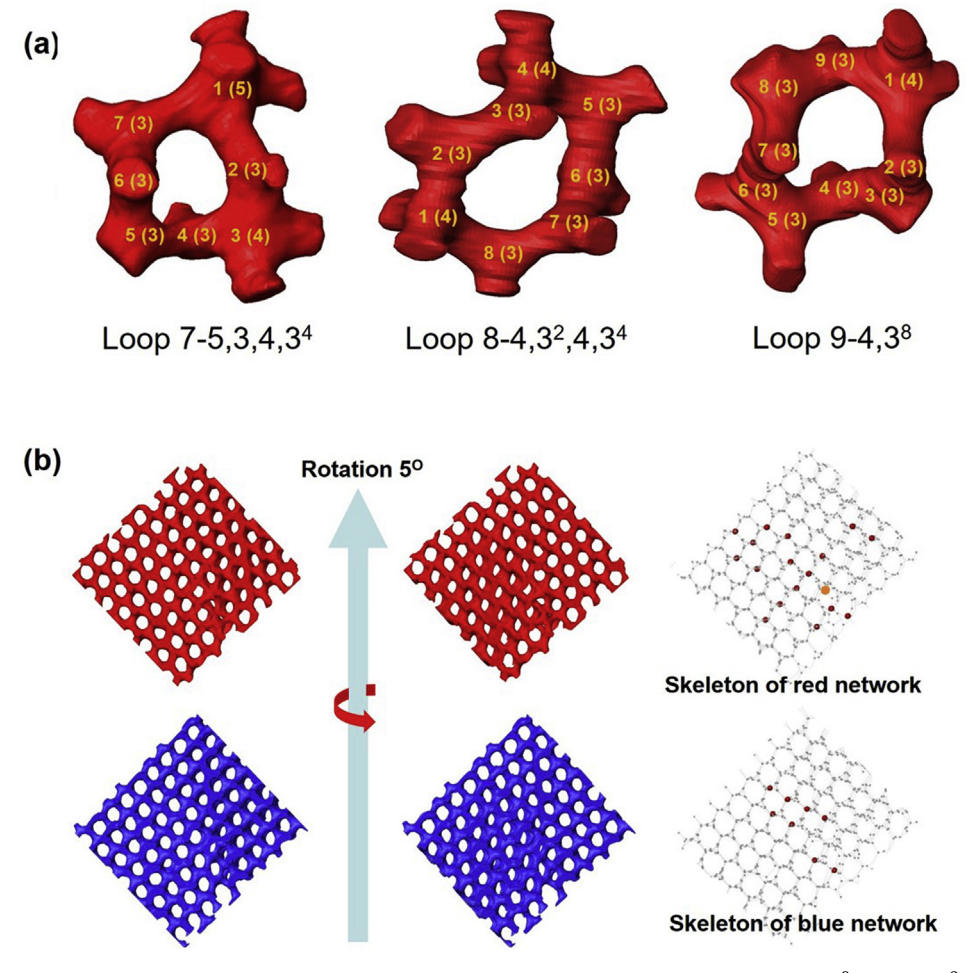


Fig. 7. (a) Loop defects have larger holes and allow threading of the 2nd gyroid network. Three examples are shown: $9-4,3^8$ loop, $8-4,3^2,4,3^4$ loop and a $7-5,3,4,3^4$ loop. (b) A group of node defects cause an approximate 5° of tilt of the two portions of the grain. The skeletal graphs of the red and blue networks are also shown. The small grey balls represent the normal f=3 nodes, the red balls represent f=4 nodes while the larger orange ball in the red network represents the single f=5 node.

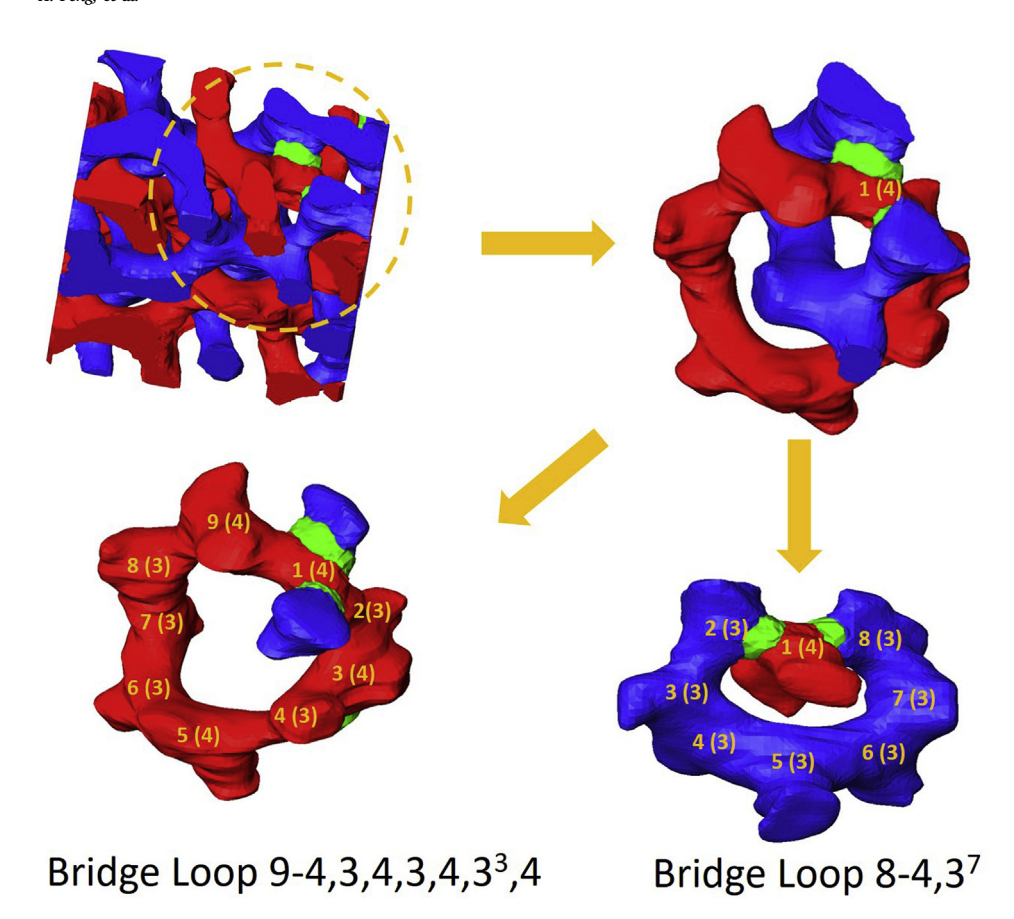


Fig. 8. Bridge defect connecting the red and blue networks at a f = 4 node. The positions where the two nets fuse are marked as green regions between the blue and red PDMS networks. The two related bridge loops are designated as $9-4,3,4,3,4,3,3^2,4$ and $8-4,3^7$; node 1(4) in the red bridge loop is also node 1(4) in the blue network.

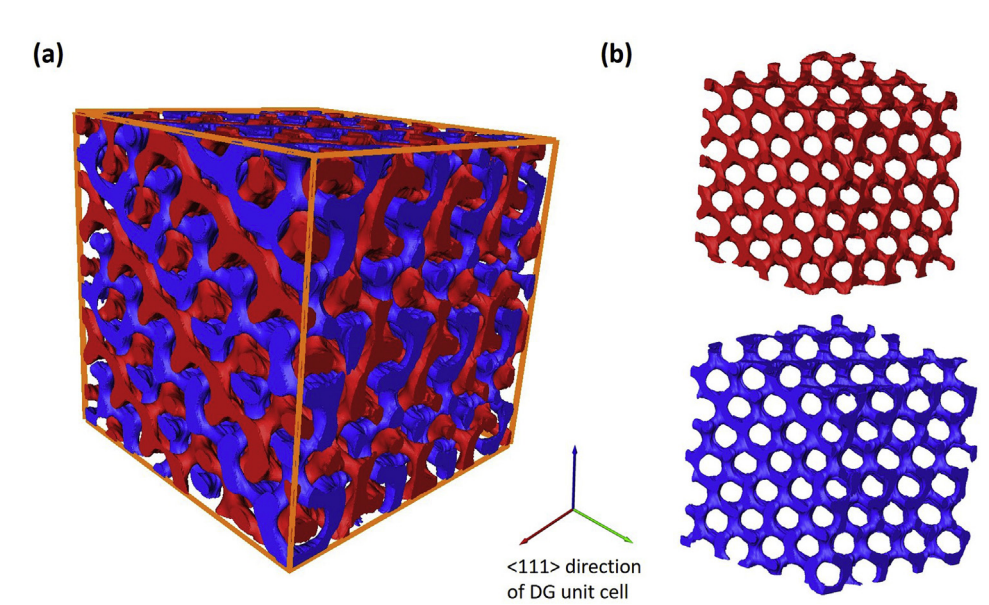


Fig. 9. (a) A defect-free volume box cropped from experimental SVSEM reconstruction with \sim 2000 nodes; (b) The IMDS of the blue and red PDMS networks from reconstruction viewed along the < 111 > direction of DG unit cell. The p6mm symmetry of the projection indicates very good long range order.

approximately \sim 2000 nodes without a single topological defect. Clearly, while TEMT and SVSEMT are different techniques and the tomograms of the DG samples examined are from different copolymers and associated sample processing/annealing, the dramatically higher number density of f defects found for the DG phase using TEM points to the limitations of the sample preparation via microtomy and the measurement technique in TEM as likely influential on the final apparent high defect content and suggests SVSEM can be a superior tool for tomographic reconstructions for BCPs.

Network defects will influence material performance and while bulk BCP self assembly has not yet reached the control afforded by 2D directed assembly [71], considering the potential exciting applications of near defect-free 3D multicontinuous materials, further efforts into the growth of large single crystals are certainly alluring. For example, the low observed value of the critical current density (J_c) of the NbN superconductor formed using a porous gyroid template may be in part due to cracks or grains of poor connectivity through the film thickness [72] and the lower maximum specific capacity of the gyroid battery

compared with its theoretical capacity could also be due to defects [20]. As has been pointed out by Wiesner et al. [73], the gyroid can exhibit negative refractive index due to the polarized plasmonic spin waves that spiral down the various helical paths in the structure. Even if large single grains of the DG phase could be grown, the spin waves would be disrupted by network breaks and joints as well as influenced by both the intra network loops and especially bridging network loops and their associated local lattice rotations. Clearly future progress in exploiting the DG structure in order to access its striking range of properties will require improved growth of more perfect self assembled materials with characterization and careful control of the various topological defects that may be present.

4. Conclusions

Topological defects in the DG network morphology were characterized by slice and view SEM to create high fidelity 3D reconstructions of a PS-PDMS diblock copolymer. We found node functionality "f defects" where the normal node functionality of 3 rose to 4 and to 5, broken network struts, bridging network struts linking the two different networks as well donut loops and defect loops comprised of 5 or 6 node rings in the former instance and 7, 8 or 9 node rings in the latter instance, instead of the characteristic 10 node ring of the ideal (10, 3)-a gyroid network. The impact of the presence of defects in the DG structure on physical properties such as electron magnetic, electron and ion transport and plasmonic spin wave propagation was discussed.

Acknowledgements

This work was supported by the National Science Foundation under the Division of Materials Research Polymers Program grant # 1742864. Helpful discussions with Prof. G. Grason, Dr. I. Prasad and Dr. C. Burke (UMASS) concerning the physics of complex phases and 3D reconstruction are highly appreciated. The advice of Mr. B. Van Leer, T. Lancon and T. Santisteban and of ThermoFisher Inc. concerning SVSEM technique and Avizo software are gratefully acknowledged. The PS-PDMS diblock was kindly synthesized and characterized by the groups of Prof. A. Avgeropoulos (Ioannina University) and Prof R-M Ho (National Taiwan University).

Appendix A. Supplementary data

Supplementary data to this article can be found online at https://doi.org/10.1016/j.polymer.2019.01.085.

References

- [1] Y.Y. Mai, A. Eisenberg, Self-assembly of block copolymers, Chem. Soc. Rev. 41 (2012) 5969–5985.
- [2] E.L. Thomas, Nanoscale 3D ordered polymer networks, Sci. China Chem. 61 (2018) 25–32.
- [3] B. Lotz, T. Miyoshi, S.Z.D. Cheng, 50th anniversary perspective: polymer crystals and crystallization: personal journeys in a challenging research field, Macromolecules 50 (2017) 5995–6025.
- [4] C.M. Bates, F.S. Bates, 50th anniversary perspective: block polymers-pure potential, Macromolecules 50 (2017) 3–22.
- [5] J.H. Lee, C.Y. Koh, J.P. Singer, S.J. Jeon, M. Maldovan, O. Stein, E.L. Thomas, 25th anniversary article: ordered polymer structures for the engineering of photons and phonons, Adv. Mater. 26 (2014) 532–568.
- [6] H. Hasegawa, T. Hashimoto, Self assembly and morphology of block copolymer systems, Compr. Polym. Sci. Suppl. 1 (1989) 497.
- [7] W.H. Li, M. Muller, Defects in the self-assembly of block copolymers and their relevance for directed self-assembly, Annu. Rev. Chem. Biomol. 6 (2015) 187–216.
- [8] Y. Fan, J.J. Walish, S.C. Tang, B.D. Olsen, E.L. Thomas, Defects, solvent quality, and photonic response in lamellar block copolymer gels, Macromolecules 47 (2014) 1130, 1136.
- [9] N.P. Balsara, H.J. Dai, H. Watanabe, T. Sato, K. Osaki, Influence of defect density on the rheology of ordered block copolymers, Macromolecules 29 (1996) 3507–3510.
- [10] S. Gupta, A. Saxena, A topological twist on materials science, MRS Bull. 39 (3) (2014) 265–279.
- [11] B.J. Dair, C.C. Honeker, D.B. Alward, A. Avgeropoulos, N. Hadjichristidis,

L.J. Fetters, M. Capel, E.L. Thomas, Mechanical properties and deformation behavior of the double gyroid phase in unoriented thermoplastic elastomers, Macromolecules 32 (1999) 8145–8152.

- [12] C.C. Honeker, E.L. Thomas, Impact of morphological orientation in determining mechanical properties in triblock copolymer systems, Chem. Mater. 8 (1996) 1702–1714.
- [13] B.J. Dair, A. Avgeropoulos, N. Hadjichristidis, M. Capel, E.L. Thomas, Oriented double gyroid films via roll casting, Polymer 41 (2000) 6231–6236.
- [14] D.J. Kinning, E.L. Thomas, J.M. Ottino, Effect of morphology on the transport of gases in block copolymers, Macromolecules 20 (1987) 1129–1133.
- [15] V.N. Urade, T.C. Wei, M.P. Tate, J.D. Kowalski, H.W. Hillhouse, Nanofabrication of double-gyroid thin films, Chem. Mater. 19 (2007) 768–777.
- [16] Z.H. Li, K. Hur, H. Sai, T. Higuchi, A. Takahara, H. Jinnai, S.M. Gruner, U. Wiesner, Linking experiment and theory for three-dimensional networked binary metal nanoparticle-triblock terpolymer superstructures, Nat. Commun. 5 (2014).
- [17] V.Z.H. Chan, J. Hoffman, V.Y. Lee, H. Iatrou, A. Avgeropoulos, N. Hadjichristidis, R.D. Miller, E.L. Thomas, Ordered bicontinuous nanoporous and nanorelief ceramic films from self assembling polymer precursors, Science 286 (1999) 1716–1719.
- [18] E.J.W. Crossland, M. Kamperman, M. Nedelcu, C. Ducati, U. Wiesner, D.M. Smilgies, G.E.S. Toombes, M.A. Hillmyer, S. Ludwigs, U. Steiner, H.J. Snaith, A bicontinuous double gyroid hybrid solar cell, Nano Lett. 9 (2009) 2807–2812.
- [19] H.Y. Hsueh, Y.C. Ling, H.F. Wang, L.Y.C. Chien, Y.C. Hung, E.L. Thomas, R.M. Ho, Shifting networks to achieve subgroup symmetry properties, Adv. Mater. 26 (2014) 3225–3229.
- [20] J.G. Werner, G.G. Rodriguez-Calero, H.D. Abruna, U. Wiesner, Block copolymer derived 3-D interpenetrating multifunctional gyroidal nanohybrids for electrical energy storage, Energy Environ. Sci. 11 (2018) 1261–1270.
- [21] M. Maldovan, A.M. Urbas, N. Yufa, W.C. Carter, E.L. Thomas, Photonic properties of bicontinuous cubic microphases, Phys. Rev. B 65 (2002).
- [22] S.Y. Peng, R.Y. Zhang, V.H. Chen, E.T. Khabiboulline, P. Braun, H.A. Atwater, Three-Dimensional single gyroid photonic crystals with a mid-infrared bandgap, ACS Photonics 3 (2016) 1131–1137.
- [23] L. Lu, L. Fu, J.D. Joannopoulos, M. Soljacic, Weyl points and line nodes in gyroid photonic crystals, Nat. Photon. 7 (2013) 294–299.
- [24] J.A. Dolan, B.D. Wilts, S. Vignolini, J.J. Baumberg, U. Steiner, T.D. Wilkinson, Optical properties of gyroid structured materials: from photonic crystals to metamaterials, Adv. Opt. Mater. 3 (2015) 12–32.
- [25] S.P. Gido, J. Gunther, E.L. Thomas, D. Hoffman, Lamellar diblock copolymer grain-boundary morphology .1. Twist boundary characterization, Macromolecules 26 (1993) 4506–4520.
- [26] S.P. Gido, E.L. Thomas, Lamellar diblock copolymer grain-boundary morphology .4. Tilt boundaries, Macromolecules 27 (1994) 6137–6144.
- [27] B.L. Carvalho, R.L. Lescanec, E.L. Thomas, Grain-boundary defects in block-copolymer systems bulk and thin-film results, Macromol. Symp. 98 (1995) 1131–1146.
- [28] Y. Nishikawa, H. Kawada, H. Hasegawa, T. Hashimoto, Grain-boundary morphology of lamellar microdomains, Acta Polym. 44 (1993) 247–255.
- [29] L. Corte, K. Yamauchi, F. Court, M. Cloitre, T. Hashimoto, L. Leibler, Annealing and defect trapping in lamellar phases of triblock terpolymers, Macromolecules 36 (2003) 7695–7706.
- [30] E.L. Thomas, D.J. Kinning, D.B. Alward, C.S. Henkee, Ordered packing arrangements of spherical micelles of diblock copolymers in 2 and 3 dimensions, Macromolecules 20 (1987) 2934–2939.
- [31] H. Jinnai, R.J. Spontal, Transmission electron microtomography in polymer research, Polymer 50 (2009) 1067–1087.
- [32] H. Jinnai, Y. Nishikawa, R.J. Spontak, S.D. Smith, D.A. Agard, T. Hashimoto, Direct measurement of interfacial curvature distributions in a bicontinuous block copolymer morphology, Phys. Rev. Lett. 84 (2000) 518–521.
- [33] H.W. Park, J. Jung, T. Chang, K. Matsunaga, H. Jinnai, New epitaxial phase transition between DG and HEX in PS-b-PI, J. Am. Chem. Soc. 131 (2009) 46–47.
- [34] C.K. Chen, H.Y. Hsueh, Y.W. Chiang, R.M. Ho, S. Akasaka, H. Hasegawa, Single helix to double gyroid in chiral block copolymers, Macromolecules 43 (2010) 8637–8644.
- [35] V.H. Mareau, S. Akasaka, T. Osaka, H. Hasegawa, Direct visualization of the perforated layer/gyroid grain boundary in a polystyrene-block-polyisoprene/polystyrene blend by electron tomography, Macromolecules 40 (2007) 9032–9039.
- [36] M. Kleman, Points, Lines and Walls in Liquid Crystals, Magnetic Systems and Various Ordered Media, Wiley, New York, 1983.
- [37] H. Matsuoka, H. Tanaka, T. Hashimoto, N. Ise, Elastic-scattering from cubic lattice systems with paracrystalline distortion, Phys. Rev. B 36 (1987) 1754–1765.
- [38] K. Saijo, G. Shin, T. Hashimoto, Y. Amemiya, K. Ito, Strain-phase-resolved dynamic SAXS studies of BCC-spherical domains in block copolymers under Laos: creation of twinned BCC-sphere and their dynamic response, Macromolecules 46 (2013) 1549–1562.
- [39] D.E. Angelescu, J.H. Waller, R.A. Register, P.M. Chaikin, Shear-induced alignment in thin films of spherical nanodomains, Adv. Mater. 17 (2005) 1878–1881.
- [40] R.A. Segalman, A. Hexemer, R.C. Hayward, E.J. Kramer, Ordering and melting of block copolymer spherical domains in 2 and 3 dimensions, Macromolecules 36 (2003) 3272–3288.
- [41] B.M. Rosen, C.J. Wilson, D.A. Wilson, M. Peterca, M.R. Imam, V. Percec, Dendron-mediated self-assembly, disassembly, and self-organization of complex systems, Chem. Rev. 109 (2009) 6275–6540.
- [42] A. Reddy, M.B. Buckley, A. Arora, F.S. Bates, K.D. Dorfman, G.M. Grason, Stable Frank-Kasper phases of self-assembled, soft matter spheres, Proc. Natl. Acad. Sci. U. S. A 115 (2018) 10233–10238.
- [43] R.J. Spontak, M.C. Williams, D.A. Agard, 3-Dimensional study of cylindrical morphology in a styrene butadiene styrene block copolymer, Polymer 29 (1988)

X. Feng, et al.

- 387-395
- [44] K. Kimishima, T. Koga, T. Hashimoto, Order-order phase transition between spherical and cylindrical microdomain structures of block copolymer. I. Mechanism of the transition, Macromolecules 33 (2000) 968–977.
- [45] J.H. Ahn, W.C. Zin, Mechanism of morphological transition from lamellar/perforated layer to gyroid phases, Macromol. Res. 11 (3) (2003) 152–156.
- [46] I. Park, B. Lee, J. Ryu, K. Im, J. Yoon, M. Ree, T. Chang, Epitaxial phase transition of polystyrene-b-polyisoprene from hexagonally perforated layer to gyroid phase in thin film, Macromolecules 38 (2005) 10532–10536.
- [47] J. Jung, J. Lee, H.W. Park, T. Chang, H. Sugimori, H. Jinnai, Epitaxial phase transition between double gyroid and cylinder phase in diblock copolymer thin film, Macromolecules 47 (2014) 8761–8767.
- [48] C.Y. Chu, W.F. Lin, J.C. Tsai, C.S. Lai, S.C. Lo, H.L. Chen, T. Hashimoto, Order-order transition between equilibrium ordered bicontinuous nanostructures of double diamond and double gyroid in stereoregular block copolymer, Macromolecules 45 (2012) 2471–2477.
- [49] A.H. Schoen, Infinite Periodic minimal surfaces without self-intersections, NASA Technical Note, NASA TN D-5541, (1970).
- [50] D.A. Hajduk, P.E. Harper, S.M. Gruner, C.C. Honeker, G. Kim, E.L. Thomas, L.J. Fetters, The gyroid - a new equilibrium morphology in weakly segregated diblock copolymers, Macromolecules 27 (1994) 4063–4075.
- [51] I. Prasad, H. Jinnai, R.M. Ho, E.L. Thomas, G.M. Grason, Anatomy of triply-periodic network assemblies: characterizing skeletal and inter-domain surface geometry of block copolymer gyroids, Soft Matter 14 (2018) 3612–3623.
- [52] K. Michielsen, D.G. Stavenga, Gyroid cuticular structures in butterfly wing scales: biological photonic crystals, J. R. Soc. Interface 5 (2008) 85–94.
- [53] S.T. Hyde, G.E. Schroder, Novel surfactant mesostructural topologies: between lamellae and columnar (hexagonal) forms, Curr. Opin. Colloid Interface Sci. 8 (2003) 5–14.
- [54] N. Politakos, E. Ntoukas, A. Avgeropoulos, V. Krikorian, B.D. Pate, E.L. Thomas, R.M. Hill, Strongly segregated cubic microdomain morphology consistent with the double gyroid phase in high molecular weight diblock copolymers of polystyrene and poly(dimethylsiloxane), J. Polym. Sci., Polym. Phys. Ed. 47 (2009) 2419–2427.
- [55] A. Avgeropoulos, B.J. Dair, N. Hadjichristidis, E.L. Thomas, Tricontinuous double gyroid cubic phase in triblock copolymers of the ABA type, Macromolecules 30 (1997) 5634–5642.
- [56] T.A. Shefelbine, M.E. Vigild, M.W. Matsen, D.A. Hajduk, M.A. Hillmyer, E.L. Cussler, F.S. Bates, Core-shell gyroid morphology in a poly(isoprene-block-styrene-block-dimethylsiloxane) triblock copolymer, J. Am. Chem. Soc. 121 (1999) 8457–8465.
- [57] X.Y. Feng, M.J. Zhuo, H. Guo, K.Q. Yang, C.J. Burke, I. Prasad, R.M. Ho, A. Avgeropoulos, G.M. Grason, E.L. Thomas, 3D Morphological Characterization of Complex Soft Matter Assemblies at the Sub-Unit Cell Level. (2019) to be submitted.
- [58] R.J. Spontak, J.C. Fung, M.B. Braunfeld, J.W. Sedat, D.A. Agard, L. Kane, S.D. Smith, M.M. Satkowski, A. Ashraf, D.A. Hajduk, S.M. Gruner, Phase behavior of

ordered diblock copolymer blends: effect of compositional heterogeneity, Macromolecules 29 (1996) 4494–4507.

Polymer 168 (2019) 44-52

- [59] J.H. Laurer, D.A. Hajduk, J.C. Fung, J.W. Sedat, S.D. Smith, S.M. Gruner, D.A. Agard, R.J. Spontak, Microstructural analysis of a cubic bicontinuous morphology in a neat SIS triblock copolymer, Macromolecules 30 (1997) 3938–3941.
- [60] C.A. Lambert, L.H. Radzilowski, E.L. Thomas, Triply periodic level surfaces as models for cubic tricontinuous block copolymer morphologies, Philos. T. R. Soc. A 354 (1996) 2009–2023.
- [61] J. Harting, M.J. Harvey, J. Chin, P.V. Coveney, Detection and tracking of defects in the gyroid mesophase, Comput. Phys. Commun. 165 (2005) 97–109.
- [62] A. Singer, L. Boucheron, S.H. Dietze, K.E. Jensen, D. Vine, I. McNulty, E.R. Dufresne, R.O. Prum, S.G.J. Mochrie, O.G. Shpyrko, Domain morphology, boundaries, and topological defects in biophotonic gyroid nanostructures of butterfly wing scales, Sci. Adv. 2 (2016).
- [63] T.Y. Lo, C.C. Chao, R.M. Ho, P. Georgopanos, A. Avgeropoulos, E.L. Thomas, Phase transitions of polystyrene-b-poly(dimethylsiloxane) in solvents of varying selectivity, Macromolecules 46 (2013) 7513–7524.
- [64] M. Cantoni, L. Holzer, Advances in 3D focused ion beam tomography, MRS Bull. 39 (2014) 354–360.
- [65] P.G. Kotula, G.S. Rohrer, M.P. Marsh, Focused ion beam and scanning electron microscopy for 3D materials characterization, MRS Bull. 39 (2014) 361–365.
- [66] D.C. Joy, C.S. Joy, Low voltage scanning electron microscopy, Micron 27 (1996) 247–263.
- [67] M. Kato, T. Ito, Y. Aoyama, K. Sawa, T. Kaneko, N. Kawase, H. Jinnai, Three-dimensional structural analysis of a block copolymer by scanning electron microscopy combined with a focused ion beam, J. Polym. Sci., Polym. Phys. Ed. 45 (2007) 677–683
- [68] Avizo User's Guide, Thermal Fisher Scientific.
- [69] A.F. Wells, Three Dimensional Nets and Polyhedra, Wiley, New York, 1977.
- [70] H. Jinnai, T. Kajihara, H. Watashiba, Y. Nishikawa, R.J. Spontak, Interfacial and topological measurements of bicontinuous polymer morphologies, Phys. Rev. E 64 (2001)
- [71] T. Segal-Peretz, J.X. Ren, S.S. Xiong, G. Khaira, A. Bowen, L.E. Ocola, R. Divan, M. Doxastakis, N.J. Ferrier, J. de Pablo, P.F. Nealey, Quantitative three-dimensional characterization of block copolymer directed self-assembly on combined chemical and topographical prepatterned templates, ACS Nano 11 (2017) 1307–1319.
- [72] S.W. Robbins, P.A. Beaucage, H. Sai, K.W. Tan, J.G. Werner, J.P. Sethna, F.J. DiSalvo, S.M. Gruner, R.B. Van Dover, U. Wiesner, Block copolymer self-assembly-directed synthesis of mesoporous gyroidal superconductors, Sci. Adv. 2 (2016)
- [73] K. Hur, Y. Francescato, V. Giannini, S.A. Maier, R.G. Hennig, U. Wiesner, Three-dimensionally isotropic negative refractive index materials from block copolymer self-assembled chiral gyroid networks, Angew. Chem. Int. Ed. 50 (2011) 11985–11989.